CD1b-restricted GEM T cell responses are modulated by Mycobacterium tuberculosis mycolic acid meromycolate chains

Chancellor, Andrew ; Tocheva, Anna S.; Cave-Ayland, Chris; Tezera, Liku; White, Andrew ; Al-Dulayymi, Juma'a; Bridgeman, John S.; Tews, Ivo; Williams, Susan ; Lissin, Nikolai M.; Tebruegge, Marc; Marshall, Ben; Sharpe, Sally ; Elliott, Tim; Skylaris, Chris-Kriton; Essex, Jonathan W.; Baird, Mark; Gadola, Stephan; Elkington, Paul; Mansour, Salah

PNAS

DOI:
10.1073/pnas.1708252114

Published: 19/12/2017

Peer reviewed version

CD1b-restricted GEM T cell responses are modulated by *Mycobacterium tuberculosis* mycolic acid meromycolate chains

Andrew Chancellor[a,b], Anna S. Tocheva[a#], Chris Cave-Ayland[c], Liku Tezera[a], Andrew White[b], Juma'a R. Al Dulayymi[d], John S. Bridgeman[e], Ivo Tews[f,g], Susan Wilson[a,h], Nikolai M. Lissin[i], Marc Tebruegge[a,g,j,k,l,m], Ben Marshall[a,g,j], Sally Sharpe[b], Tim Elliott[g,n], Chris-Kriton Skylaris[c,g], Jonathan W. Essex[c,g], Mark S. Baird[d], Stephan Gadola[a,g,o], Paul Elkington[a,g,j,k], Salah Mansour[a,g,1]

[a]Academic Unit of Clinical and Experimental Sciences, Faculty of Medicine, Southampton SO16 6YD, UK

[b]Public Health England, National Infections Service, Porton Down, Salisbury, SP4 0JQ, UK

[c]School of Chemistry, University of Southampton, Southampton SO17 1BJ, UK

[d]School of Chemistry, Bangor University, Bangor, Gwynedd LL57 2UW, UK

[e]Cellular Therapeutics Ltd, Manchester M13 9XX, UK

[f]School of Biological Sciences, University of Southampton, Southampton, SO17 1BJ, UK

[g]Institute for Life Sciences, University of Southampton, Southampton SO17 1BJ, UK

[h]Histochemistry Unit, University of Southampton, Southampton, SO16 6YD, UK

[i]Immunocore Limited, Abingdon, Oxon OX14 4RY, United Kingdom

[j]NIHR Southampton Biomedical Research Centre, Southampton, UK SO17 1BJ, UK

[k]Global Health Research Institute, University of Southampton, Southampton, SO17 1BJ, UK

[l]Department of Paediatrics, Faculty of Medicine, University of Melbourne, 3052 Parkville, Australia

[m]Department of Paediatric Infectious Diseases & Immunology, Evelina London Children's Hospital, Guy's and St. Thomas' NHS Foundation Trust, London, SE1 7EH, UK

[n]Cancer Sciences Unit, Faculty of Medicine, University of Southampton, Southampton, UK SO16 6YD, UK

[o]F.Hoffmann-La Roche Ltd, Basel, Switzerland

[#]New address: Department of Medicine, New York University School of Medicine, New York, NY 10016, USA

[1]To whom correspondence should be addressed: s.mansour@soton.ac.uk

Key words

CD1b, mycolate, *Mycobacterium tuberculosis*, GEM T cells

Abstract

Tuberculosis, caused by *Mycobacterium tuberculosis*, remains a major human pandemic. Germline-encoded mycolyl lipid-reactive (GEM) T cells are donor-unrestricted and recognize CD1b-presented mycobacterial mycolates. However, the molecular requirements governing mycolate antigenicity for the GEM T cell receptor (TCR) remain poorly understood. Here, we demonstrate CD1b expression in tuberculosis granulomas and reveal a central role for meromycolate chains in influencing GEM-TCR activity. Meromycolate fine structure influences T cell responses in TB-exposed individuals, and meromycolate alterations modulate functional responses by GEM-TCRs. Computational simulations suggest that meromycolate chain dynamics deep within CD1b regulate mycolate head group movement, thereby modulating GEM-TCR activity. Our findings have significant implications for the design of future vaccines that target GEM T cells.

Significance statement

Tuberculosis is a major global pandemic responsible for more deaths than any other infectious disease, yet no effective vaccine exists. Here we demonstrate CD1b expression within human tuberculous granulomas, supporting a role for CD1b lipid antigen presentation in host immunity to infection. CD1b presents mycolates, the dominant Mtb cell wall lipid class and key virulence factors, to αβ T cells. We reveal that mycolate tail moieties, buried deep within CD1b, are antigenic determinants for the conserved human germline-encoded mycolyl lipid-reactive (GEM) T cell receptors (TCRs). Computational simulations suggest a putative mechanism whereby lipid-ligand dynamics within CD1b regulate GEM TCR activity. This work provides insights for the development of MHC-independent Mtb lipid vaccines, including those that target GEM T cells.

\body

Introduction

Tuberculosis (TB), caused by *Mycobacterium tuberculosis* (Mtb), remains a major human pandemic and is responsible for more deaths than any other infectious disease (1). The only licensed vaccine, Bacille Calmette-Guérin (BCG), provides very limited protection against adult TB that leads to transmission (2), and therefore new strategies to control the disease are needed. Immunological responses considered critical for long-term mycobacterial control have focused on conventional T cell responses directed at peptide antigens presented by major histocompatibility complex (MHC) I and II, ultimately leading to secretion of anti-microbial cytokines, including TNF-α and IFN-γ (3, 4). A number of subunit vaccines based on immunogenic peptides have been developed, some of which have been evaluated in clinical trials, but results to date have not been encouraging (5-7).

Mtb is characterized by a lipid-rich envelope that comprises diverse and unique lipid structures (8). Multiple Mtb lipids are presented by CD1 proteins to lipid-reactive αβ T cells, which are increasingly being recognised as important components of the host immune response (9-13). The CD1 family comprises five non-polymorphic MHC class-I-like proteins, CD1a, CD1b, CD1c, CD1d and CD1e, which present lipid-antigens to T cells at the surface of antigen presenting cells (APC), with the exception of CD1e (14). CD1b has the capacity to bind various Mtb lipid antigens, including mycolates (15), sulfoglycolipids (16), lipoarabinomannan (LAM) and phosphatidylinositol mannoside (PIM) (17). CD1b-restricted T cells responsive to mycobacterial lipids secrete anti-mycobacterial cytokines, such as IFN-γ and TNF-α, supporting their potential role in the host immune response to Mtb infection (9, 18). In humanized mice, CD1b-restricted T cells generate polyfunctional responses which reduce mycobacterial proliferation *in vitro* and accumulate in mycobacteria-induced lung granulomas *in vivo* (19). Furthermore, CD1b-restricted polycytotoxic T cells in bronchioalveolar fluid were recently shown to limit Mtb growth *ex vivo* (20). In TB patients, CD1b-restricted T cell numbers in peripheral blood and at the site of infection expand and contract markedly according to pathogen burden, and therefore may contribute to the immune response to Mtb (18). Taken together, this evidence suggests that T cell responses directed to Mtb lipids presented by CD1b are important for Mtb containment.

Mycolates are a major lipid component of the Mtb cell wall and are key virulence factors (21). They comprise long chain β-hydroxy fatty acids, composed of a shorter unfunctionalised α-alkyl chain and a longer meromycolate chain that typically has two functional groups, providing the main source of structural diversity (Fig. S1*A*). Three major mycolate classes exist in Mtb, including α-, keto- and methoxy-, based on functional groups within the meromycolate chain, which are proximal or distal to the head group moiety (Fig. S1*A*) (22). In addition, mycolates occur with different chain lengths, and stereo-arrangements of functional groups, generating a large spectrum of possible mycolate structures. Mycolates may exist as free

mycolic acid (MA), which can be esterified to glycerol (Gro-MM), glucose (GMM) or trehalose (TMM) (Fig. S1*B-D*). MA, Gro-MM and GMM are all CD1b-presented lipid antigens (22-24). When bound to CD1b, the meromycolate chain positions itself within the long A', T' and F' super channel of CD1b, while the shorter α-alkyl chain occupies the C' channel, via hydrophobic interactions (25). The hydrophilic head group is exposed above the F' portal, thus contributing directly to the T cell receptor (TCR) interface (25).

Knowledge of the CD1b-mycolate specific T cell compartment has until recently been based on a few isolated clones that may not accurately represent the T cell repertoire *in vivo* (9, 26). More recently, CD1b-tetramers have been developed to efficiently capture GMM-specific T cells (9). Emerging data now suggest a pattern of TCR conservation, revealing two T cell compartments that differ in their binding affinity to CD1b. The germline-encoded mycolyl lipid-reactive T cells (GEMs) express a conserved TCR and respond to Mtb infection by clonal expansion and secretion of anti-mycobacterial cytokines (9). GEM TCRs, which are defined by their TRAV1-2 usage, bind to GMM-loaded CD1b with high affinity. Depending on TCR β-chain usage, GEMs can recognise MA or GMM (9). The second compartment contains the semi-invariant LDN5-like T cells, including LDN5, a T cell clone bearing a TCR that binds CD1b-GMM with moderate affinity (27). Therefore, donor-unrestricted GEM T cells, that are activated by mycolic acids presented by non-polymorphic CD1b molecules, are potentially powerful targets for future vaccines or diagnostics that may be effective in the majority of the human population.

A central tenet of CD1b-restricted TCR recognition of mycolates is the fine discrimination of the glycolipid head group moiety (27). However, the major source of mycolate diversity is derived from structural determinants within the meromycolate chain which are distal to the head group moiety (22). This feature has not been systematically investigated in relation to T cell activation. We hypothesized that these structural variations may modulate the activation of CD1b-restricted T cells. We reveal GEM-TCR sensitivity to meromycolate chain functional group structure and stereo-arrangement. Molecular simulations of CD1b-MA complexes show marked differences in mycolate behaviour, which is related to meromycolate chain interactions with the binding groove of CD1b. Our findings reveal that activation of GEM-TCRs by mycolates is finely tuned by meromycolate chain structure, which could be exploited for future vaccine or diagnostic approaches.

Results

CD1b is expressed in human pulmonary TB granulomas

CD1b is expressed in leprosy lesions that exhibit protective immunity (28, 29), whereas it has been reported that CD1b is downregulated on the cell surface of $CD1^+$ APCs infected with Mtb *in vitro* (30). To investigate CD1b expression in human granulomas, we performed immunohistochemical staining of lung biopsies from five patients with active pulmonary TB. Many of the cells in the granulomas were positive for the macrophage marker CD68, with diffuse positive staining within caseous necrosis (Fig. 1*A* and Fig. S2). CD1b was expressed within the majority of granulomas stained, with immunoreactive cells situated primarily adjacent to the central caseous core (Fig. 1*B* and Fig S2 *B, D, E, F, J, K*). Negative control stains confirmed absence of non-specific antibody binding (Fig. 1*C* and Fig S2 *C, G, H, I, L, M*). Quantitation of immunoreactive cells in 5 granuloma areas per biopsy showed a range of CD1b expression (Median and IQR: 6 +/- 10.5 cells/mm^2). Diffuse foci of CD1b immunoreactivity were also observed within the caseous necrosis (Fig. S3). These results confirm CD1b expression at the site of infection, in line with previous reports demonstrating upregulation of CD1b in human mycobacterial infection (28, 29), and consistent with a role for CD1b-mediated presentation of Mtb lipids to T cells in the host immune response.

GEM18 TCR exhibits promiscuous mycolate head group specificity

Mycolates comprise a structurally diverse species of Mtb cell wall lipids which can activate CD1b-restricted human T cells (9, 26), including GEM T cells (9, 26). However, antigenic determinants of mycobacterial mycolates for CD1b-restricted T cells have not been fully defined. To investigate this, we generated human J.RT3.T3-5 and NFAT-GLuc Jurkat T cells stably expressing the mycolate-specific TCRs, GEM clone 1 (GEM1), GEM clone 18 (GEM18), and LDN5 (9, 26). Jurkat T cells expressing TCR were activated by CD1b in the presence of mycolate, whereas no activation occurred in the absence of either the TCR, CD1b or mycolate (Fig. 2*A*). To examine the fine specificity of these TCRs to different mycolates, we investigated their reactivity to JR1080, an α-MA, as free MA or when esterified to glycerol, glucose or trehalose head group moieties (Fig. 2*B*). GEM1- and LDN5-TCRs were specific for GMM (Fig. 2*C-E*) and did not respond to MA, Gro-MM or TMM. In contrast, the GEM18-TCR recognised MA and Gro-MM, as well as GMM to a lesser extent, but did not respond to TMM (Fig. 2*E*). Similar to a previous report (31), our results demonstrate the promiscuity of GEM18-TCR toward mycolate head group moieties. This suggests that meromycolate chain structure might be an antigenic determinant for GEM18-TCR activity.

Meromycolate chain functional groups dictate GEM-TCR activity

We next investigated the role of meromycolate chain structure on GEM-TCR activity using a panel of synthetic mycolates. MA derived from pathogenic bacteria such as Mtb generally have distal and proximal functional groups in the long meromycolate chain, defined by X and Y respectively (Fig. S1*A*). Functional groups include cyclopropane, methoxy, keto, epoxy, diene and alkene moieties (Table S1). We first assessed GEM18-TCR activity to a panel of 12 synthetic MAs that all comprise the same short α-alkyl chains of C_{23} or C_{21}, but diverse meromycolate chains containing different functional groups at various locations, including the Mtb MAs JR1080, AD129, JRRR124, MH140, JR1046, and JRRR121 (Fig. 3 and Table S1). Initial dose-response studies showed that 10 μg/ml of MA was optimal to investigate T cell activation. Stimulation of GEM18 Jurkat T cells with a panel of MAs at 10 μg/ml revealed a distinct hierarchy for GEM18-TCR activation (Fig. 3*A*, *B*). A luminescence-based NFAT-GLuc T cell activation assay confirmed this pattern (Fig. S4*A*). Strong T cell activation was mediated by the diene mycolic acid MH157, a MA not expressed by Mtb (Table S1) (32). Of the Mtb mycolates, JR1080 induced the strongest T cell activation, which matched the stereochemistry of the expected major Mtb α-mycolate, based on a common biosynthetic pathway for all three major MA classes (33, 34). This effect was significantly greater than with the other α-MAs tested, such as MMS131 and MMS130, which are not expressed by Mtb (Table S1). AD129, matching the chain lengths and expected stereochemistry of the major keto-MA of Mtb, caused moderate activity, as did JRRR124, matching the expected structure and stereochemistry of the major methoxy-MA. The keto-MA MH140, matching the corresponding *trans*-cyclopropane, caused minimal activation, as did the corresponding *trans*-cyclopropane containing methoxy-MA, JRRR121.

Stereoarrangements of meromycolate chain functional groups are a naturally occurring feature of structural diversity. Therefore, to assess whether the stereochemistry of meromycolate functional groups influenced GEM-TCR activity, we investigated stereoisomers of JR1080, matching the chain lengths of the most abundant Mtb α-MA (Table S1) (33). This revealed an activation hierarchy dependent on stereochemistry and identified CDL12DU as a more potent antigen of GEM18-TCR than JR1080, at concentrations as low as 0.1 μg/ml (Fig. 3*C* and Fig. S4*B*). Next, we investigated GEM18-TCR reactivity against a panel of synthetic Gro-MMs, containing diverse meromycolate chains. GEM18 responded in a hierarchical, dose dependant manner to three of the six Gro-MMs, based on analysis of CD69 upregulation (Fig. 3*D*) and luminescence (Fig. S4*C*). In addition, five Gro-MMs displayed a similar activation pattern as MAs containing the same meromycolate chains (Fig. S4*D* and Table S1). We further assessed the activation of Jurkat T cells expressing GEM1-, GEM18-, and LDN5-TCRs toward a panel of GMMs that comprise similar C_{23} or C_{21} short α-alkyl chains but structurally variable meromycolate chains (Fig. S5*A* and Table S1). We observed differences in GEM18-TCR activation toward these GMMs (Fig. S5*B, E*). In contrast, minor differences in T cell activation occurred for GEM1-TCR (Fig. S5*C, F*), and no differences were observed for LDN5-TCR towards these GMMs (Fig. S5*D*). Taken together, these results demonstrate that the functional

group type, position and relative stereoarrangement within the meromycolate chain strongly impact on GEM18-TCR activity.

Mtb mycolates modulate functional human T cell responses

We next determined whether meromycolate structural differences affected activation of human peripheral blood T cells from Mtb-exposed individuals. We co-cultured MA-loaded autologous $CD1b^+$ monocyte derived dendritic cells (moDC) with peripheral blood lymphocytes from ten patients with latent TB infection. Intracellular cytokine staining was performed for IL-2^+, IFN-γ^+ and TNF-α^+ in activated T lymphocytes. Strong T cell activation was observed with the MA JR1080 and the GMM SMP74, while the MAs MMS130 and JRRR121 were weakly-stimulatory (Fig. 4*A*). Significantly more cells produced detectable levels of IL-2, IFN-γ, and TNF-α following stimulation with JR1080 compared with JRRR121, and in the majority of patients JRRR121 and MMS130 did not activate any T cells.

To overcome limitations associated with low numbers of CD1b reactive T cells in the periphery *ex vivo* (9, 35), we transferred the GEM18-TCR into *ex vivo* derived T cell populations, for high levels of expression to study functional impact (Fig. S6*A*). T cell function was measured after co-culture of GEM18-expressing T cells with $CD1b^+$ T2 lymphoblasts loaded with three strongly-stimulatory (CDL12DU, JR1080, DZ146) and three weakly-stimulatory MAs (JRRR121, MMS130, JR1046). JR1080 exhibited significantly increased cell killing in each case when compared to the non-stimulatory ligands (JRRR121 p=0.0003, MMS130 p=0.006, JR1046 p=<0.0001 [Fig. 4*B*]). The same was also true of CDL12DU (JRRR121 p=0.0096, MMS130 p=0.02 and JR1046 p=0.018). We also measured functional cytokine responses, studying pro-inflammatory and anti-inflammatory cytokines known to be critical in anti-mycobacterial immunity (3). Immunogenic MA induced higher levels of IFN-γ secretion by GEM18-expressing T cells than any of the non-stimulatory mycolates (Fig. 4*C*). Particularly strong responses were noted for IFN-γ, GM-CSF, IL-2 and TNF-α, which were statistically significant in all cases (Fig. 4*D* and Fig. S6*B*).

GEM18-TCR exhibits differential binding to CD1b-MA complexes

We next investigated binding of GEM18-TCR to CD1b molecules treated with MA meromycolate variants. We first produced soluble recombinant GEM18-TCR (Fig. 5*A*) and soluble fluorescent GEM18-TCR dextramers. To investigate GEM18-TCR dextramer binding, we used a recently reported CD1b loading protocol of methoxy MA developed by Van Rhijn et al. (36), utilising the least hydrophobic lipids in our panel. We treated CD1b coated beads with three MA that induced differential activity of GEM18-TCR in Jurkat cellular assays (Fig. 3*B*). Staining of MA treated CD1b-beads with GEM18-TCR dextramers revealed a distinct hierarchy of fluorescence intensity (Fig. 5*B*), which correlated to the results observed in Jurkat

activation assays. In addition, we treated CD1b monomers with the strongly-stimulatory methoxy MA HA56 and the weaker methoxy MA JRRR124 and then generated soluble fluorescent CD1b-dextramers. Jurkat T cells expressing GEM18-TCR were positively stained by CD1b-dextramers treated with the strongly-stimulatory MA HA56, and with lower staining intensity by CD1b-dextramers treated with the weaker JRRR124 (Fig. 5*C*). CD1b-dextramers treated with MA failed to stain Jurkat T cells expressing irrelevant CD1d or CD1c restricted TCRs. Together, these findings support the concept that the differential responses induced by MA variants are mediated either through differential lipid loading or via a direct TCR-CD1b binding mechanism.

Meromycolate chain anchoring modulates MA antigenicity

Next, we hypothesized that the differential activity of mycolates upon GEM-TCR activation might be due to mechanisms related to lipid behaviour within the antigen-binding groove of CD1b. To determine whether structural alterations in regions of the ligand that are distal to the carboxylate head group might be communicated to the surface of the CD1b-ligand complex that interfaces with the TCR, we performed molecular dynamics simulations for CD1b bound to highly-stimulatory and weakly-stimulatory mycolates. Over the trajectory time course, we examined the position and behaviour of the MA head group with different meromycolate chain substitutions. Head group position was measured via the distance moved in reference to the head group of GMM in the existing crystal structure of CD1b-GMM complex (25). Root mean squared deviation (RMSD) values were calculated to provide a measure of structural similarity to the putative productive conformation of CD1b-GMM. These simulations showed that JR1080 adopts similar conformations to the head group of CD1b-GMM, whereas the weakly-stimulatory JRRR121 adopts markedly different conformations (Fig. 6*A*). These observations show a substantial increase in overall head group movement in the weakly-stimulatory MA JRRR121 (Movies S1, S2).

Study of the meromycolate chains were then carried out through visualization and comparison of substituent centroids, indicating the geometric centre of functional group positions over the trajectory time period. Marked differences in centroid localization and dynamics were apparent between stimulatory and weakly-stimulatory MAs. The weakly-stimulatory MAs JRRR121 and JR1046 showed much more pronounced localization of centroids, in the T' tunnel (distal, red) and A' channel (proximal, blue) (Fig 6*B* and Fig S7), whereas the strongly stimulatory MAs MH157 and JR1080 showed greater fluidity (Fig. 6*C* and Fig S7). Chain fluidity was further investigated to understand differences in this behaviour. In instances of strong localisation, this was found to be due to interaction of chain substituents with features of the CD1b binding pocket. For example, the JRRR121 proximal and distal chain substituents are strongly localised by their respective interactions with small crevices of the A’ and T' tunnels, thereby resulting in an “anchoring”

mechanism (Movies S3, S4). This strongly suggests that the different dynamic behaviour of ligands within the binding pocket is determined by the position and properties of long chain substituents.

Discussion

TCRαβ$^+$ CD1b-restricted mycolate-specific GEM lymphocytes are a conserved T cell population in humans which expand upon Mtb infection and exhibit potent anti-mycobacterial effector functions through production of IFN-γ and TNF-α (9, 31, 37, 38). Our demonstration of CD1b expression within human lung TB granulomas provides further evidence for lipid-specific T cell immunity in host defence against TB. CD1b is an attractive target for the development of TB vaccines due to its non-polymorphic nature. However, development of such vaccines requires a precise understanding of the antigenic determinants for CD1b-presented mycolates that are recognised by GEM-TCRs. Using a panel of synthetic pure mycolates, we dissected the role of different structural features in defining recognition and functional responses by GEM TCRs. Our studies reveal a major and unexpected role for structural determinants in the meromycolate chain, distal to the carboxylate head group moiety and not expected to bind the TCR based on CD1b-GMM structures, in defining T cell activity.

The concept that deeply buried moieties of CD1-bound lipids can influence T cell activation is supported by several studies. For example, the alkyl chains of Mtb diacylated sulfoglycolipids (AC_2SGL) govern CD1b-mediated T cell activity, including C-methyl substituents, stereochemistry and alkyl chain position (39). T cell activation is also sensitive to alkyl chain differences in the CD1c-antigen mannosyl-β-phosphomycoketide (MPM), with length, methyl branching pattern and stereoarrangments influencing responses (40). Furthermore, the length of the alkyl chains and lipid saturation of the CD1d-antigen α-galactosylceramide (α-GalCer) is important for controlling CD1d-restricted invariant NKT cell activity (41). Consistent with these reports, our data suggest that communication of structural differences in lipid tails to T cells is a central feature of CD1-lipid antigen presentation. Our findings suggest a mechanism for TCR-ligand interaction, which may also be generalizable for ligand recognition by CD1c and CD1d molecules. It may also contribute to the fine-tuning of classical peptide-MHC recognition by TCR (42).

We employed molecular dynamics simulations of MAs to gain a mechanistic understanding for how subtle differences within these lipid structures may impact on the potency of the T cell response. These analyses supported the notion that ligand dynamics within the CD1b pocket can be strongly influenced by meromycolate chain substituents. Based on these *in silico* insights and our experimental data, we propose a model whereby meromycolate chain dynamics within the CD1b groove are directly linked to the ability of the hydrophilic head group to adopt productive conformations for TCR binding. In this model, weakly stimulatory lipids with immobile tails are 'trapped' due to the position and nature of their chain substituents, and this trapping consequently restricts the head group from adopting positions that facilitate

TCR binding. In contrast, strongly stimulatory lipids have chain substituents that do not 'catch' on pocket features and as such are more readily accommodated by the binding pocket. This manifests as greater chain mobility, thereby allowing the head group to adopt productive conformations for TCR binding. Thus, ligand-dynamics have the potential to fine tune GEM T cell recognition and therefore function.

Structural studies of GEM42-TCR in complex with CD1b-GMM recently provided a molecular mechanism for GMM recognition by so called "typical" GMM specific GEM-TCRs such as GEM1, GEM21, and GEM42 (31). Arg107α on the CDR3α loop cooperates with Asp113β on the CDR3β loop forming a salt bridge that acts as a capstone, stabilising the alpha and beta 'tweezers' that grip the glucose head group moiety of GMM (31). This highly rigid and specific mechanism for gripping the glucose moiety likely contributes toward the insensitivity of such TCRs toward meromycolate changes. Furthermore, contacts between Arg79 and Thr157 found in the α1 and α2 helices and GMM may stabilize the head group, which may counter any movement due to a lack of backbone anchoring (25). On the other hand, GEM18-TCR differs from typical GMM-recognizing GEM-TCRs in that it possesses a Leu107α residue instead of Arg107α on its CDR3α loop, and Asp113β is absent, therefore GEM18-TCR lacks the stabilising 'tweezers' (31). The promiscuity toward different mycolate head groups suggests that GEM18-TCR recognises a common mycolate epitope that is shared between MA, GMM, and Gro-MM, likely mediated by Gly110α and Phe112α within the CDR3α loop (31). The observed weak GEM18-TCR responses toward GMM could have resulted through interference from the relatively bulky glucose moiety; however, we could not definitively rule out the processing of GMM to MA post cellular uptake. In addition, our results could not rule out the possibility that MA variants may have altered loading or TCR recognition. Definitive conclusions must await structural determination of GEM18-TCR with CD1b mycolate complexes.

Different strains of Mtb and other mycobacteria express significantly different MA structural profiles and Mtb is known to considerably change its MA composition in response to different growth conditions and virulence stages (22, 43, 44). It is therefore essential to understand the structure-function relationships of Mtb-derived mycolates using synthetic lipids due to the complex mixtures and difficulty in isolating a single natural molecule. Indeed, an earlier study investigating the response of DN1 TCR hinted on a diverse role for MA structural variants on T cell activity (45). Furthermore, our results are consistent with data from a recent study by Van Rhijn et al. (36) indicating that MA lipid tails are antigenic determinants for T cells. Therefore, an emerging concept is that individual MAs should be considered as distinct lipid antigens that may elicit diverse activation profiles by diverse MA-specific TCRs. It is tempting to speculate that the differential activity of MA on CD1b restricted TCR may provide a means for Mtb to modulate the host immune response during infection. Consequently, manipulating mycolate structure could be a key strategy to generate optimal anti-mycobacterial responses for future vaccines. Functional differences between lipids were most pronounced for cytokine release relative to cytotoxicity, likely reflecting the latter being a more downstream effect. Defining the ability of GEMs and other mycolate specific T cells to detect different

meromycolate structures *in vivo* and characterizing their role in immunity to Mtb are key areas warranting further investigation.

In conclusion, we report a systematic investigation of mycobacterial meromycolate chain structure in regulating CD1b-restricted GEM T cell activity. The fine sensitivity of the conserved GEM-TCR for subtle meromycolate changes and the co-evolution of humans and Mtb over the last 70,000 years suggests an intricate role in protection against mycobacterial infection (46). We provide insights into the molecular antigenic determinants for GEM-TCR activation and our findings may inform future vaccination strategies that harness the potential of donor-unrestricted T cells to control the ongoing TB pandemic.

Materials and Methods

Immunohistochemistry

Paraffin-embedded Mtb-infected human lung tissue was retrieved from the histology archive at University Hospital Southampton with approval by the Institutional Review Board (Reference 12/NW/0794 SRB04_14). Sections (4 μm thick) were dewaxed, rehydrated and endogenous peroxidase blocked. Heat induced-epitope retrieval was performed. Non-specific staining was blocked and primary antibodies applied overnight at 4°C (anti-CD1b mouse monoclonal SN13; K5 1B8-Abcam 1:50; CD68 mouse monoclonal ED1-LifeSpan Bioseciences, 1:200). Negative control sections were incubated with buffer alone. Secondary goat anti-mouse antibody for CD1b, CD68 and the negative control was used at 1:800. Sections were developed with avidin biotin-peroxidase complexes (Elite vectastain ABC kit, Vector laboratories), and 3,3'-diaminobenzidine tetrahydrochloride (DAB) (2-component DAB pack, BioGenex). Slides were counterstained with Mayer's haematoxylin, dehydrated, cleared, mounted in pertex and dried, then imaged on an Olympus BX51, CC12 DotSlide microscope. Slides were digitised using an Olympus VS-110 digital slide scanner running Olympus VS-ASW-L100 acquisition software. The number of immunoreactive cells within the granulomas were counted and granuloma area was measured using Image J software with BIOP plugin and results presented as cells mm^{-2}.

Cloning

CD1b Construct: MoDCs were lyzed with Trizol (Invitrogen) and RNA was precipitated. cDNA was synthesized using superscript III first strand synthesis with random primers (Invitrogen). For PCR of the CD1b sequences, the following primers were used: 1. forward primer 5'-GCGCGCTAGCCGCCACCATGCTGCTGCTGCCATTTCAACTGTTAGC-'3, 2. reverse primer 5'-

GCGCGTCGACTCATGGGATATTCTGATATGACC-'3. CD1b sequences were subsequently digested and cloned into the third-generation pELNS lentivector kindly provided by James Riley (University of Pennsylvania).

TCR Constructs: The publically available GEM18-TCRα (TRAV1-2, accession JQ778258.1) and TCRβ (TRBV6-2, accession JQ778257.1) chain sequences (9) were synthesized by GeneArt (Thermo Fisher) and sub-cloned into the pELNS lentivector. The TCRβ-chain (TRBV30, accession JQ778264.1) of GEM1-TCR was synthesized and cloned into the GEM18-cassette; replacing the GEM18 TRBV6-2 sequence. Site-directed mutagenesis was subsequently performed on the TCRα-chain to yield a complete GEM1 TCRα sequence (TRAV1-2, accession JQ778263.1), using the following primers: forward 5'-GCCGTGCGGGTCACCGGCGGCT-3', reverse 5'-AGCCGCCGGTGACCCGCACGGC-3'. LDN5-TCRα and TCRβ (TRAV17/TRBV4-1) was cloned as previously described (47).

Generating transgenic cell lines: Lentiviruses encoding CD1b or TCRs were generated in HEK293TN cells after co-transfection of three accessory plasmids; pCMV-VSV-G (1.5 μg), pRSV.REV (3 ug), and pMDL.pg.RRE (3 μg) in combination with engineered pELNS lentivector (2.5 μg) (48). Lentiviral particles were harvested, filtered and used directly for transduction of T2 lymphoblasts, J.RT3.T3-5 and NFAT-GLuc Jurkat T cell lines. Transduced cells were sorted by flow cytometry on a FACSAria (BD Biosciences). For primary T cell transduction, lentiviral particles were harvested, concentrated, filtered, and then added to enriched T cells previously cultured overnight with anti-CD28 and anti-CD3 antibody coated Dynabeads (Thermo Fisher). Cells were then expanded for two weeks, before staining with anti-TRAV1-2 (clone 3C10) antibody to assess transduction efficiency on a FACSCalibur (BD Biosciences).

Mycolic Acid preparation and formulation

MA and their sugar esters were prepared as described previously (32, 49-54). Table S1 provides structural information. Chemically synthesized MA were dried, then resuspended at 1 mg/ml in 9:1 chloroform/methanol, aliquoted, evaporated and then frozen at -20°C for future use. When required, the aliquots were resuspended in complete media and sonicated for 30 minutes at 80°C before use.

DC generation

Blood was obtained from asymptomatic donors with latent tuberculosis diagnosed by positive interferon-gamma release assay (QuantiFERON-TB Gold In-Tube assay; Cellestis/Qiagen). Peripheral blood mononuclear cells (PBMC) were isolated by density gradient centrifugation using Ficoll-Hypaque (GE Healthcare). Monocytes were positively selected by anti-CD14 magnetic microbeads (Miltenyi Biotec) and differentiated into moDCs in complete media (RPMI 1640 supplemented with 1% L-glutamine, 1%

penicillin/streptomycin and 10% fetal calf serum (FCS) (all Lonza)) and 25 ng/ml GM-CSF and 20 ng/ml IL-4 (Miltenyi Biotec) for 5 days. CD1b expression was confirmed by flow cytometry.

T cell assays

Activation of Jurkat T cells: T2 lymphoblasts were pulsed with lipid for 16 h and then cultured with Jurkat T cell lines in a 1:1 ratio in a 96-well plate. After a further 18 h, Jurkat activation was measured by determining CD69 (clone FN50) upregulation by flow cytometry. Activation of NFAT-GLuc Jurkat T cells was measured using the Gaussia luciferase kit (New England Biolabs) as per manufacturer's instructions. GLuc assay solution was added to cell culture supernatant in a 96-well plate (Corning) and luminescence was read (Glo-max Discover, Promega).

Intracellular cytokine staining: Monocyte-depleted T cell fractions were rapidly thawed, and allowed to recover before addition of autologous moDC pulsed with 5 μg/ml lipid in a ratio of 1:2 in a 96-well plate. The culture was incubated at 37°C for 6 h in the presence of 2.5 μg/ml anti-CD28, 10 μg/ml brefeldin A and 1x monensin (Biolegend). Cells were then transferred to flow cytometry tubes for intracellular cytokine staining. Positive controls were incubated with phorbol ester (PMA) and ionomycin at 50 ng/ml and 500 ng/ml respectively.

T cell stimulation: GEM18-TCR transduced T cells were thawed rapidly and recovered in complete media for 4 h. Cells were then washed and added to lipid pulsed T2 lymphoblasts in a ratio of 1:2 for 24 h in a total volume of 200μl in a 96-well plate. After activation, supernatant was removed for cytokine analysis using xMAP assays (R & D systems) and cell viability was directly assessed using Cytotox-glo cytotoxicity assay (Promega) according to manufacturer's instructions, with luminescence measured by Glo-Max Discover (Promega) after 15 minutes. Then 30 μg/ml digitonin was added to wells to assess total cell death.

Luminex xMAP assays: Concentrations of cytokine were determined using a Bioplex 200 platform (Bio-Rad) according to the manufacturer's protocol. Cytokines analyzed included: IL-2, IL-4, IL-6, IL-8, IL-10, IL-12(p70), IL-17a, TNF-α, IFN-γ and GM-CSF (R & D systems).

Soluble TCR and TCR dextramers: Generation of TCR heterodimers were performed as previously described (47). Briefly, the extracellular domains of TCRα and TCRβ chains were produced in *E.coli* Rosetta as inclusion bodies after cloning into the bacterial expression vector pGMT7. To produce stably refolded disulphide-linked heterodimers, cysteines were incorporated into the TCRα- and β-chain constant domains, by replacing Thr48 and Ser57, respectively. The disulphide-linked GEM18-TCR αβ heterodimers were expressed, refolded, and purified as previously described (47). Refolded and purified TCR was assessed by a reducing and non-reducing SDS/PAGE gel analysis. Precision Plus Protein Prestained Standard (Bio-Rad) was used as a reference molecular weight (MW) marker. GEM18-TCR dextramers were produced using modified

TCRβ chains, containing a C terminus BirA-tag motif, which was specifically biotinylated. Biotinylated TCR was subsequently purified by size-exclusion chromatography before conjugation to dextran-PE (Immudex) to generate fluorescently labelled TCR-dextramers

MA treated CD1b beads and dextramers: Soluble biotinylated CD1b monomers (Immudex) were treated with methoxy MA similar to a previously published method (36). Briefly, MA were solubilised in 100µl 50mM citrate buffer pH 4.5 containing 0.6% CHAPS detergent (Sigma) after sonication in a water bath for 2 hours at 40°C. For beads, solubilised MA were incubated with CD1b coated MACSibeads (Miltenyi) at 37°C overnight. Beads were washed in PBS containing 2% FCS before staining with GEM18-TCR dextramer. For CD1b-dextramers, 20µg of CD1b monomer was added directly to the sonicated lipid and incubated overnight at 37°C. Treated CD1b monomers were subsequently neutralized with 1M Tris buffer pH 8.5 and incubated with dextran-PE to generate soluble fluorescent CD1b-dextramers.

Flow Cytometry

The following fluorescent reagents were used: anti-CD69-PE (FN50), anti-CD3-APC (UCHT3), anti-CD3-APC-Cy7 (UCHT3), anti-CD161-APC (HP-3G10), anti-IFN-γ-PeCy7 (BS.4S), anti-IL-2-PE (JES6-5H4), anti-TNF-α-Violet-510 (MP6-XT22), anti-CD1b-APC (SN13; K-5B), and anti-TRAV1-2-PE (3C10) (all Biolegend), GEM18-TCR dextramer-PE and CD1b-MA-dextramer-PE. After addition of staining reagents, cells or beads were incubated for 45 minutes at 4°C, then washed with PBS containing 2mM EDTA. For ICS, cells were then fixed and permeabilized for 20 minutes at 4°C in the dark (BD Cytofix/cytoperm kit) before addition of intracellular fluorochrome-conjugated antibodies. Cells or beads were acquired on a FACSCalibur or FACSAria (BD Biosciences). Fixable live/dead-Violet 450 (Zombie Violet) (Biolegend) or propidium iodide (Sigma) were used to exclude dead cells. Data was analyzed using Flowjo software version 9.7.6 (Treestar).

Molecular Dynamics Simulations

A crystal structure of CD1b in complex with a GMM is available (PDB code: 1UQS)(25), however the low resolution (3.1 Å) prevented its direct use as a simulation starting structure. A 2.26 Å resolution structure (PDB code: 1GZQ) containing CD1b in complex with a phosphatidylinositol (55) was therefore used to provide the initial geometry of the CD1b and $ß_2$-microglobulin chains. Initial ligand structures were generated with the flexible alignment tool of the MOE software package (56) using the 1UQS GMM ligand as a template. The GMM α-alkyl chain of 1UQS is shorter (C_8) compared to the presently considered MA's (C_{21}-C_{23}). This left an ambiguity in the placement of the acyl chain that was resolved by allowing the chain to exit the pocket through a nearby portal of the C' channel under the apex of the α2 helix, exposing ~5-7 carbons to solvent. Preliminary simulation work with this system showed this initial binding pose to be

unstable, the solvent exposed chain rapidly re-entering the binding pocket. An observed stable pose emerging from the preliminary work was selected as a basis for the simulation results reported here.

Molecular Dynamics simulations were performed using the Amber 14 software package (57) with the ff99SB forcefield. The protein ligand complex was solvated in a box of 91x84x68 Å using the TIP3P water model and neutralized through the addition of 7 Na^+ ions. Bond lengths were constrained using the SHAKE algorithm, allowing use of a 2 fs time step. Simulations were conducted at 300 K using a Langevin thermostat with a collision frequency of 3 ps^{-1}. Where relevant below, pressure was regulated using a Monte Carlo barostat with volume moves attempted every 100 time steps. All systems were initially equilibrated with protein and ligand heavy atom restraints to preserve secondary structure elements. All systems were gradually heated from 100 to 300 K over 0.5 ns. The system volume was then allowed to equilibrate for 2 ns under NPT dynamics. The system was then cooled over 0.1 ns, and the previous process repeated with restraints on protein backbone heavy atoms only. Protein backbone restraints were then removed and the system equilibrated for a further 2 ns at 300 K.

Statistical analysis

GraphPad prism version 7.00 (GraphPad Software Inc.) was used for statistical analysis, and *p* values ≤0.05 were considered statistically significant. Mann-Whitney U test or One-Way ANOVA were used as stated in figure legends. The heat map was generated in R software package.

Acknowledgments

We thank Richard Jewell and Carolann McGuire for their assistance with flow cytometry (FACS facility, Faculty of Medicine, University of Southampton), Jenny Norman in the Histochemistry Research Unit for undertaking the immunohistochemical staining, and Sanjay Jogai for providing the reagents for immunohistochemistry. Special thanks to Joseph Sanderson, Andrew Gerry and Bent Jakobsen for advice and support for generating GEM-TCR transduced T cell lines. We also thank Liselotte Brix, Andreas Fløe Nielsen, and Bjarke Endel Hansen for generous provision of dextran backbone, CD1b monomers, and support in generating soluble fluorescent dextramers. Many thanks to Akul Singhania for production of the heat map and for statistical support. This work was supported by Public Health England, the US National Institute for Health R33AI102239, the UK Medical Research Council MR/N006631/1, and Cancer Research UK A23562.

476

477

478

479 **References**

480 1. Wallis RS*, et al.* (2016) Tuberculosis--advances in development of new drugs, treatment regimens,
481 host-directed therapies, and biomarkers. *The Lancet. Infectious diseases* 16(4):e34-46.
482 2. Nguipdop-Djomo P, Heldal E, Rodrigues LC, Abubakar I, & Mangtani P (2016) Duration of BCG
483 protection against tuberculosis and change in effectiveness with time since vaccination in Norway:
484 a retrospective population-based cohort study. *Lancet Infect Dis* 16(2):219-226.
485 3. O'Garra A*, et al.* (2013) The immune response in tuberculosis. *Annual review of immunology*
486 31:475-527.
487 4. Jasenosky LD, Scriba TJ, Hanekom WA, & Goldfeld AE (2015) T cells and adaptive immunity to
488 Mycobacterium tuberculosis in humans. *Immunol Rev* 264(1):74-87.
489 5. Tameris MD*, et al.* (2013) Safety and efficacy of MVA85A, a new tuberculosis vaccine, in infants
490 previously vaccinated with BCG: a randomised, placebo-controlled phase 2b trial. *Lancet*
491 381(9871):1021-1028.
492 6. Ndiaye BP*, et al.* (2015) Safety, immunogenicity, and efficacy of the candidate tuberculosis vaccine
493 MVA85A in healthy adults infected with HIV-1: a randomised, placebo-controlled, phase 2 trial. *The*
494 *lancet. Respiratory medicine* 3(3):190-200.
495 7. Karp CL, Wilson CB, & Stuart LM (2015) Tuberculosis vaccines: barriers and prospects on the quest
496 for a transformative tool. *Immunol Rev* 264(1):363-381.
497 8. Brennan PJ & Nikaido H (1995) The envelope of mycobacteria. *Annu Rev Biochem* 64:29-63.
498 9. Van Rhijn I*, et al.* (2013) A conserved human T cell population targets mycobacterial antigens
499 presented by CD1b. *Nat Immunol* 14(7):706-713.
500 10. Kasmar AG*, et al.* (2011) CD1b tetramers bind alpha beta T cell receptors to identify a
501 mycobacterial glycolipid-reactive T cell repertoire in humans. *Journal of Experimental Medicine*
502 208(9):1741-1747.
503 11. Rosat JP*, et al.* (1999) CD1-restricted microbial lipid antigen-specific recognition found in the CD8+
504 alpha beta T cell pool. *Journal of immunology* 162(1):366-371.
505 12. Moody DB*, et al.* (2000) CD1c-mediated T-cell recognition of isoprenoid glycolipids in
506 Mycobacterium tuberculosis infection. *Nature* 404(6780):884-888.
507 13. Matsunaga I & Sugita M (2012) Mycoketide: a CD1c-presented antigen with important implications
508 in mycobacterial infection. *Clinical & developmental immunology* 2012:981821.
509 14. Brigl M & Brenner MB (2004) CD1: antigen presentation and T cell function. *Annual review of*
510 *immunology* 22:817-890.
511 15. Moody DB*, et al.* (2000) CD1b-mediated T cell recognition of a glycolipid antigen generated from
512 mycobacterial lipid and host carbohydrate during infection. *The Journal of experimental medicine*
513 192(7):965-976.
514 16. Gilleron M*, et al.* (2004) Diacylated sulfoglycolipids are novel mycobacterial antigens stimulating
515 CD1-restricted T cells during infection with Mycobacterium tuberculosis. *The Journal of*
516 *experimental medicine* 199(5):649-659.
517 17. Ernst WA*, et al.* (1998) Molecular interaction of CD1b with lipoglycan antigens. *Immunity* 8(3):331-
518 340.
519 18. Montamat-Sicotte DJ*, et al.* (2011) A mycolic acid-specific CD1-restricted T cell population
520 contributes to acute and memory immune responses in human tuberculosis infection. *J Clin Invest*
521 121(6):2493-2503.
522 19. Zhao J*, et al.* (2015) Mycolic acid-specific T cells protect against Mycobacterium tuberculosis
523 infection in a humanized transgenic mouse model. *eLife* 4.

20. Busch M*, et al.* (2016) Lipoarabinomannan-Responsive Polycytotoxic T Cells Are Associated with Protection in Human Tuberculosis. *Am J Respir Crit Care Med* 194(3):345-355.
21. Vander Beken S*, et al.* (2011) Molecular structure of the Mycobacterium tuberculosis virulence factor, mycolic acid, determines the elicited inflammatory pattern. *European journal of immunology* 41(2):450-460.
22. Verschoor JA, Baird MS, & Grooten J (2012) Towards understanding the functional diversity of cell wall mycolic acids of Mycobacterium tuberculosis. *Progress in lipid research* 51(4):325-339.
23. Beckman EM*, et al.* (1994) Recognition of a lipid antigen by CD1-restricted alpha beta+ T cells. *Nature* 372(6507):691-694.
24. Sekanka G, Baird M, Minnikin D, & Grooten J (2007) Mycolic acids for the control of tuberculosis. *Expert Opin Ther Pat* 17(3):315-331.
25. Batuwangala T*, et al.* (2004) The crystal structure of human CD1b with a bound bacterial glycolipid. *Journal of immunology* 172(4):2382-2388.
26. Van Rhijn I*, et al.* (2014) TCR Bias and Affinity Define Two Compartments of the CD1b-Glycolipid-Specific T Cell Repertoire. *J Immunol*.
27. Moody DB*, et al.* (1997) Structural requirements for glycolipid antigen recognition by CD1b-restricted T cells. *Science* 278(5336):283-286.
28. Inkeles MS*, et al.* (2016) Cell-type deconvolution with immune pathways identifies gene networks of host defense and immunopathology in leprosy. *JCI Insight* 1(15):e88843.
29. Sieling PA*, et al.* (1999) CD1 expression by dendritic cells in human leprosy lesions: correlation with effective host immunity. *J Immunol* 162(3):1851-1858.
30. Stenger S, Niazi KR, & Modlin RL (1998) Down-regulation of CD1 on antigen-presenting cells by infection with Mycobacterium tuberculosis. *Journal of immunology* 161(7):3582-3588.
31. Gras S*, et al.* (2016) T cell receptor recognition of CD1b presenting a mycobacterial glycolipid. *Nature communications* 7:13257.
32. Taher SG, Muzael M, Al Dulayymi JR, & Baird MS (2015) Synthetic trehalose esters of cis-alkene and diene alpha'-mycolic acids of Mycobacteria. *Chemistry and physics of lipids* 189:28-38.
33. Don Lawson C, Maza-Iglesias M, Sirhan MM, Al Dulayymi JR, & Baird MS (2017) The Synthesis of Single Enantiomers of α-Mycolic Acids of Mycobacterium- tuberculosis and Related Organisms, with Alternative- Cyclopropane Stereochemistries. *SynOpen* 01(01):0103-0116.
34. Yuan Y & Barry CE, 3rd (1996) A common mechanism for the biosynthesis of methoxy and cyclopropyl mycolic acids in Mycobacterium tuberculosis. *Proceedings of the National Academy of Sciences of the United States of America* 93(23):12828-12833.
35. Seshadri C*, et al.* (2015) T Cell Responses against Mycobacterial Lipids and Proteins Are Poorly Correlated in South African Adolescents. *J Immunol* 195(10):4595-4603.
36. Rhijn IV*, et al.* (2017) CD1b-mycolic acid tetramers demonstrate T- cell fine specificity for mycobacterial lipid tails. *Eur J Immunol*.
37. Van Rhijn I & Moody DB (2015) Donor Unrestricted T Cells: A Shared Human T Cell Response. *Journal of immunology* 195(5):1927-1932.
38. Huang S & Moody DB (2016) Donor-unrestricted T cells in the human CD1 system. *Immunogenetics* 68(8):577-596.
39. Guiard J*, et al.* (2009) Fatty acyl structures of mycobacterium tuberculosis sulfoglycolipid govern T cell response. *Journal of immunology* 182(11):7030-7037.
40. de Jong A*, et al.* (2007) CD1c presentation of synthetic glycolipid antigens with foreign alkyl branching motifs. *Chemistry & biology* 14(11):1232-1242.
41. McCarthy C*, et al.* (2007) The length of lipids bound to human CD1d molecules modulates the affinity of NKT cell TCR and the threshold of NKT cell activation. *The Journal of experimental medicine* 204(5):1131-1144.
42. Hawse WF*, et al.* (2014) TCR scanning of peptide/MHC through complementary matching of receptor and ligand molecular flexibility. *J Immunol* 192(6):2885-2891.
43. Flores-Valdez MA, Morris RP, Laval F, Daffe M, & Schoolnik GK (2009) Mycobacterium tuberculosis modulates its cell surface via an oligopeptide permease (Opp) transport system. *FASEB journal :*

official publication of the Federation of American Societies for Experimental Biology 23(12):4091-4104.
44. Watanabe M, Aoyagi Y, Ridell M, & Minnikin DE (2001) Separation and characterization of individual mycolic acids in representative mycobacteria. *Microbiology* 147(Pt 7):1825-1837.
45. Grant EP*, et al.* (2002) Fine specificity of TCR complementarity-determining region residues and lipid antigen hydrophilic moieties in the recognition of a CD1-lipid complex. *Journal of immunology* 168(8):3933-3940.
46. Gagneux S (2012) Host-pathogen coevolution in human tuberculosis. *Philosophical transactions of the Royal Society of London. Series B, Biological sciences* 367(1590):850-859.
47. Mansour S*, et al.* (2016) Cholesteryl esters stabilize human CD1c conformations for recognition by self-reactive T cells. *Proc Natl Acad Sci U S A*.
48. Dull T*, et al.* (1998) A third-generation lentivirus vector with a conditional packaging system. *J Virol* 72(11):8463-8471.
49. Al Dulayymi JaR*, et al.* (2014) Synthetic trehalose di- and mono-esters of α-, methoxy- and keto-mycolic acids. *Tetrahedron* 70(52):9836-9852.
50. Al Kremawi DZ, Al Dulayymi JaR, & Baird MS (2014) Synthetic epoxy-mycolic acids. *Tetrahedron* 70(40):7322-7335.
51. Ali HM*, et al.* (2016) The synthesis of single enantiomers of trans-alkene containing mycolic acids and related sugar esters. *Tetrahedron* 72(45):7143-7158.
52. Ali OT, Sahb MM, Al Dulayymi JaR, & Baird MS (2017) Glycerol mycolates from synthetic mycolic acids. *Carbohydrate Research* 448:67-73.
53. Koza G*, et al.* (2013) The synthesis of methoxy and keto mycolic acids containing methyl-trans-cyclopropanes. *Tetrahedron* 69(30):6285-6296.
54. Sahb MM, Al Dulayymi JaR, & Baird MS (2015) Glucose monomycolates based on single synthetic mycolic acids. *Chemistry and physics of lipids* 190:9-14.
55. Gadola SD*, et al.* (2002) Structure of human CD1b with bound ligands at 2.3 A, a maze for alkyl chains. *Nature immunology* 3(8):721-726.
56. Anonymous (2017) Molecular Operating Environment (MOE) (Chemical Computing Group Inc, Chemical Computing Group Inc., 1010 Sherbooke St. West, Suite #910, Montreal, QC, Canada, H3A 2R7).
57. Case DA*, et al.* (2016) AMBERUniversity of California, San Francisco).

Figure Legends

Fig 1 CD1b expression within human TB granulomas**.** Human lung biopsies from patients with confirmed TB were stained for (*A*) the macrophage marker CD68 and (*B*) CD1b. (*C*) Negative control with secondary antibody and ABC detection only. Scale bar (*A, B, C*) 200μm. Box; magnified insert.

Fig 2 Cross reactivity of GEM18-TCR. (*A*) Representative flow cytometry plots showing GEM18-TCR activation through upregulation of CD69 (y-axis) on Jurkat T cells. GEM18-TCR transduced Jurkat T cells, but not mock transduced Jurkat T cells, upregulate CD69 when cultured with $CD1b^+$ T2 lymphoblasts in the presence of the MA JR1080 (Table S1). Phorbol ester PMA and ionomycin (PMA/Iono) was used as positive control. (*B*) Structure of free mycolic acid (MA) JR1080 and its glycerol monomycolate (Gro-MM) OTA-23, glucose monomycolate (GMM) SMP74, and trehalose monomycolate (TMM) MH176 studied in (*C-E*). (*C*) Activation of GEM1, (*D*) LDN5, and (*E*) GEM18 Jurkat T cell lines cultured with $CD1b^+$ T2 lymphoblasts in the presence of MA (JR1080), Gro-MM (OTA-23), GMM (SMP74), TMM (MH176), or no antigen (No Ag). Data are representative of at least three independent experiments (*C, D, E*; mean and s.e.m of duplicate measurements).

Fig 3 Meromycolate chain structure determines GEM18-TCR activity. (*A*) Representative flow cytometry plots of CD69 expression on GEM18 Jurkat T cell lines cultured with $CD1b^+$ T2 lymphoblasts in the presence of no antigen (No Ag), weakly-stimulatory MA (JRRR121) and strongly-stimulatory MA (JR1080). (*B*) Activation of GEM18 Jurkat T cells cultured with $CD1b^+$ T2 lymphoblasts in the presence of various MA at 10 μg/ml that contain different meromycolate chain structures. (*C*) Activation of GEM18 Jurkat T cells when cultured with $CD1b^+$ T2 lymphoblasts in the presence of MAs that represent the cyclopropane stereoisomers of the Mtb α-MA (JR1080). Stimulations performed in a dose response, with TMM (MH176) as the negative control. (*D*) Activation of GEM18 Jurkat T cells cultured with $CD1b^+$ T2 lymphoblasts in the presence of Gro-MM that contain different meromycolate chain structures. Stimulations performed in a dose response, with TMM (MH176) as the negative control. Structures of lipids are shown next to the graphs. All graphs are representative of at least three independent experiments performed in duplicate; mycolate concentrations were; 0.1 μg/ml (clear), 1 μg/ml (light grey), 10 μg/ml (dark grey), 20 μg/ml (black), (*B, C, D*; mean and s.e.m of duplicate measurements).

Fig 4 Mycolic acid meromycolate variants induce diverse functional responses. (*A*) *Ex vivo* T cells from human TB patients were stimulated with autologous monocyte derived DC (moDC) in the presence of one strongly-stimulatory MA (JR1080) and GMM (SMP74) or the weakly-stimulatory MAs (JRRR121, MMS130). Intracellular IL-2, IFN-γ and TNF-α were measured by flow cytometry. Cells were pre-gated on $CD3^+$, $CD161^-$, live lymphocytes. Cytokine positive cells are plotted relative to negative control. (*B*) Cell viability of GEM18 transduced ex vivo T cells cultured with $CD1b^+$ T2 lymphoblasts in the presence of indicated MA. Targeted cell killing was assessed using Cytotox-Glo

assay. (*C*) Absolute values of IFN-γ cytokine secretion from GEM18 transduced ex vivo T cells cultured with $CD1b^+$ T2 lymphoblasts in the presence of indicated MA. Cytokine secretion was measured by luminex array. (*D*) Heat map summarizing luminex array data showing relative concentrations of cytokines in response to lipid antigen. Values were normalized to the mean cytokine concentrations measured in supernatants following stimulation with weakly-stimulatory MAs. Red indicates high concentrations, blue low concentrations. Data representative of three independent experiments performed in triplicate. * p <0.05 ***p<0.001, ****p<0.0001 (*A*; Mann-Whitney U test, *B, C*; One-Way ANOVA). (*B, C*; mean and s.d of duplicate measurements).

Fig 5 Differential binding of GEM18-TCR to soluble CD1b monomers treated with MAs. (*A*) SDS/PAGE analysis of recombinant GEM18-TCR under reducing (R) and non-reducing (NR) conditions. The predicted molecular weights of the TCRα and TCRβ monomeric proteins and for TCRαβ heterodimeric proteins are indicated. (*B*) GEM18-TCR dextramer binding to MACSibeads conjugated to CD1b treated with the methoxy MAs JRRR121, JRRR124, and HA56. Untreated CD1b MACSibeads were used as control. (*C*) Specific staining of Jurkat T cells expressing GEM18-TCR with CD1b dextramers treated with weakly-stimulatory (JRRR124) and strongly-stimulatory (HA56) methoxy MAs. HA56 loaded CD1b dextramer binding of Jurkats expressing CD1d (iNKT) and CD1c (NM4) restricted TCRs are shown as background controls.

Fig 6 Meromycolate chain immobilization affects ligand head group dynamics. (*A*) Root mean square deviation (RMSD) value for mycolic acid head group movement relative to head group of GMM in previously determined CD1b-GMM complex (1UQS). Higher RMSD values indicate conformations less similar to that observed in 1UQS, whilst a greater spread of values indicates increased mobility of ligand head group. Vertical bars mark mean values for histograms of the corresponding colour. Highly-stimulatory antigens have a lower mean RMSD, while the less stimulatory antigens have a higher mean RMSD. (*B, C*) Geometric functional group positions are indicated by centroids (coloured balls). Data was generated from 200ns molecular dynamic simulations. (*B*) Representative weakly-stimulatory ligands (JRRR121 and JR1046) and (*C*) strongly-stimulatory ligands (JR1080 and MH157). Position of proximal (blue) and distal (red) functional groups are shown.

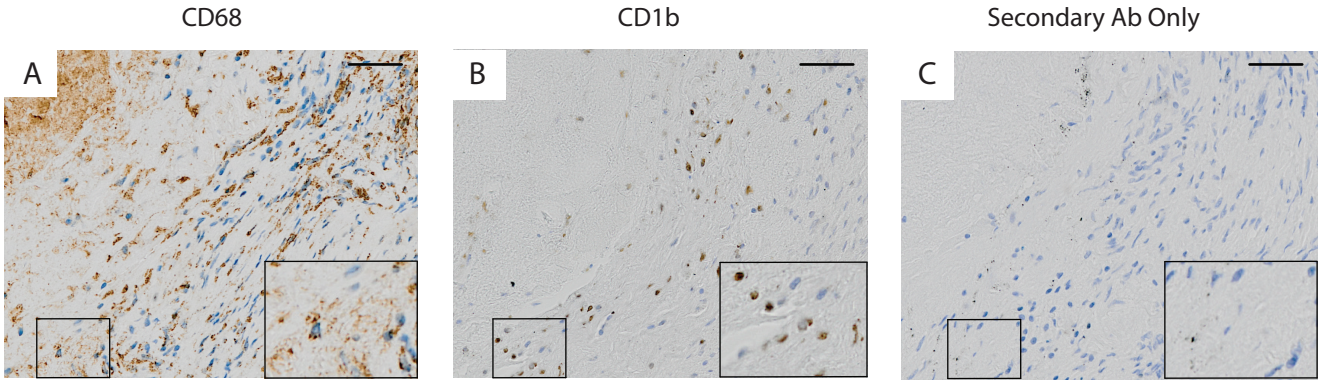
CD68
CD1b
Secondary Ab Only
A
B
C

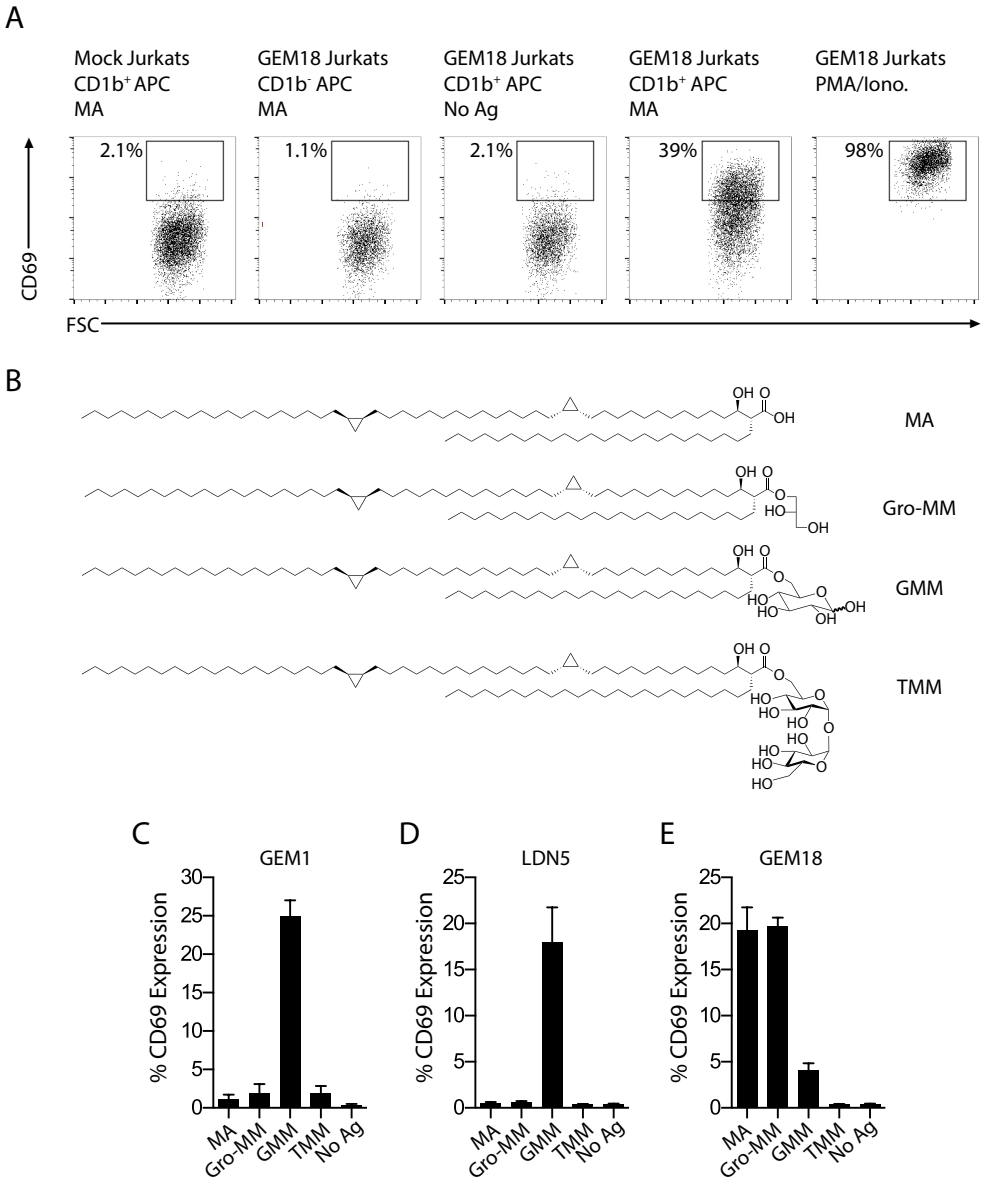
A
Mock Jurkats
CD1b+ APC
MA
GEM18 Jurkats
CD1b- APC
MA
GEM18 Jurkats
CD1b+ APC
No Ag
GEM18 Jurkats
CD1b+ APC
MA
GEM18 Jurkats
PMA/Iono.
2.1%
1.1%
2.1%
39%
98%
CD69
FSC
B
MA
Gro-MM
GMM
TMM
C
GEM1
D
LDN5
E
GEM18
% CD69 Expression
MA
Gro-MM
GMM
TMM
No Ag

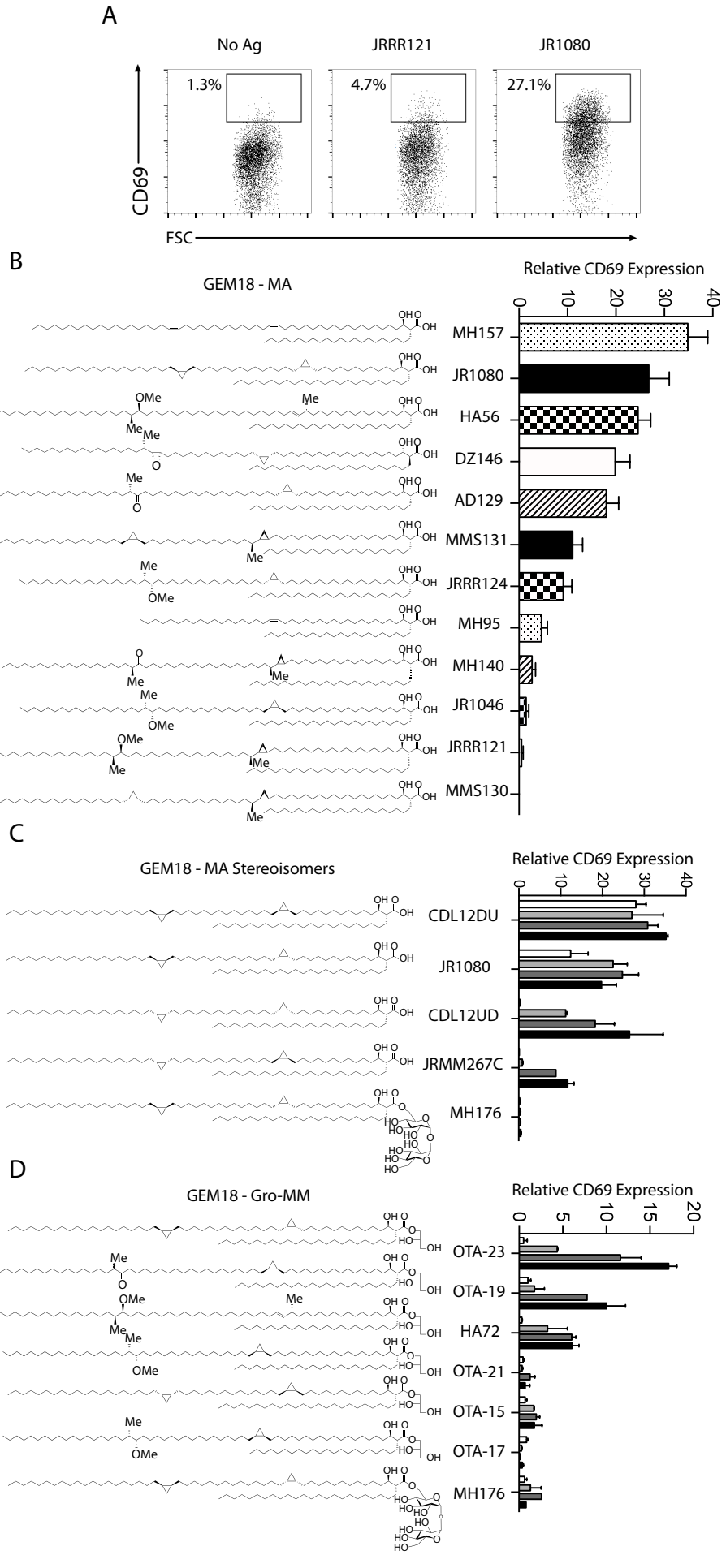
A
No Ag
JRRR121
JR1080
1.3%
4.7%
27.1%
CD69
FSC
B
GEM18 - MA
Relative CD69 Expression
0
10
20
30
40
MH157
JR1080
HA56
DZ146
AD129
MMS131
JRRR124
MH95
MH140
JR1046
JRRR121
MMS130
C
GEM18 - MA Stereoisomers
Relative CD69 Expression
0
10
20
30
40
CDL12DU
JR1080
CDL12UD
JRMM267C
MH176
D
GEM18 - Gro-MM
Relative CD69 Expression
0
5
10
15
20
OTA-23
OTA-19
HA72
OTA-21
OTA-15
OTA-17
MH176

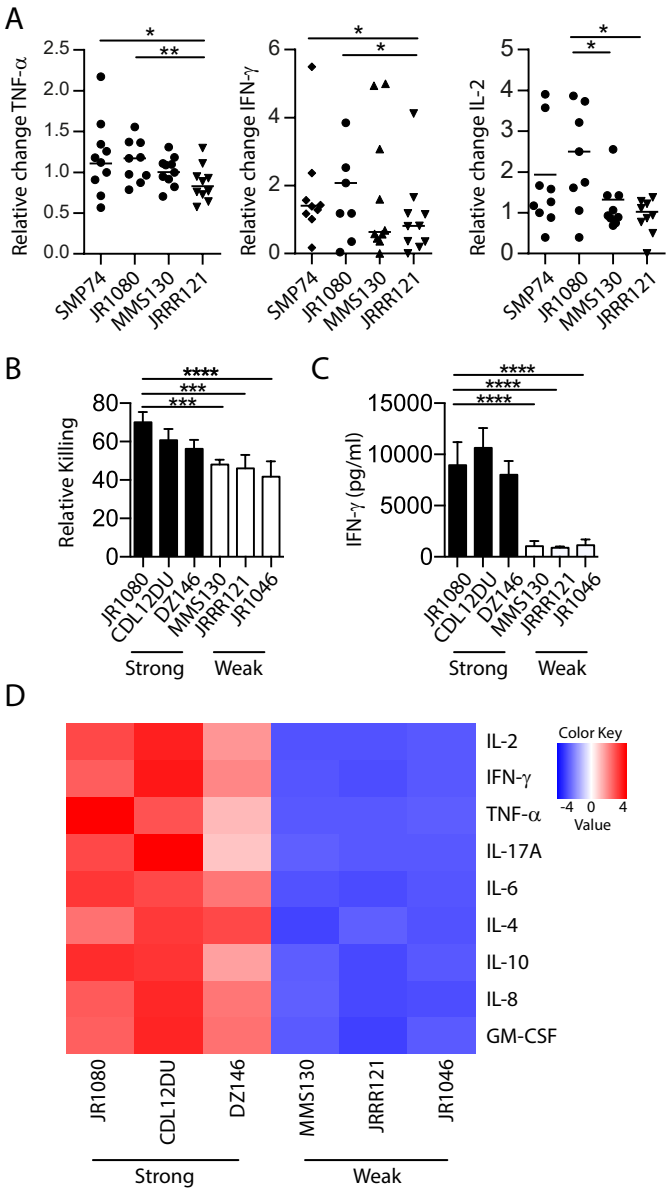
A
Relative change TNF-α
Relative change IFN-γ
Relative change IL-2
SMP74
JR1080
MMS130
JRRR121
B
Relative Killing
C
IFN-γ (pg/ml)
JR1080
CDL12DU
DZ146
MMS130
JRRR121
JR1046
Strong
Weak
D
IL-2
IFN-γ
TNF-α
IL-17A
IL-6
IL-4
IL-10
IL-8
GM-CSF
Color Key
Value

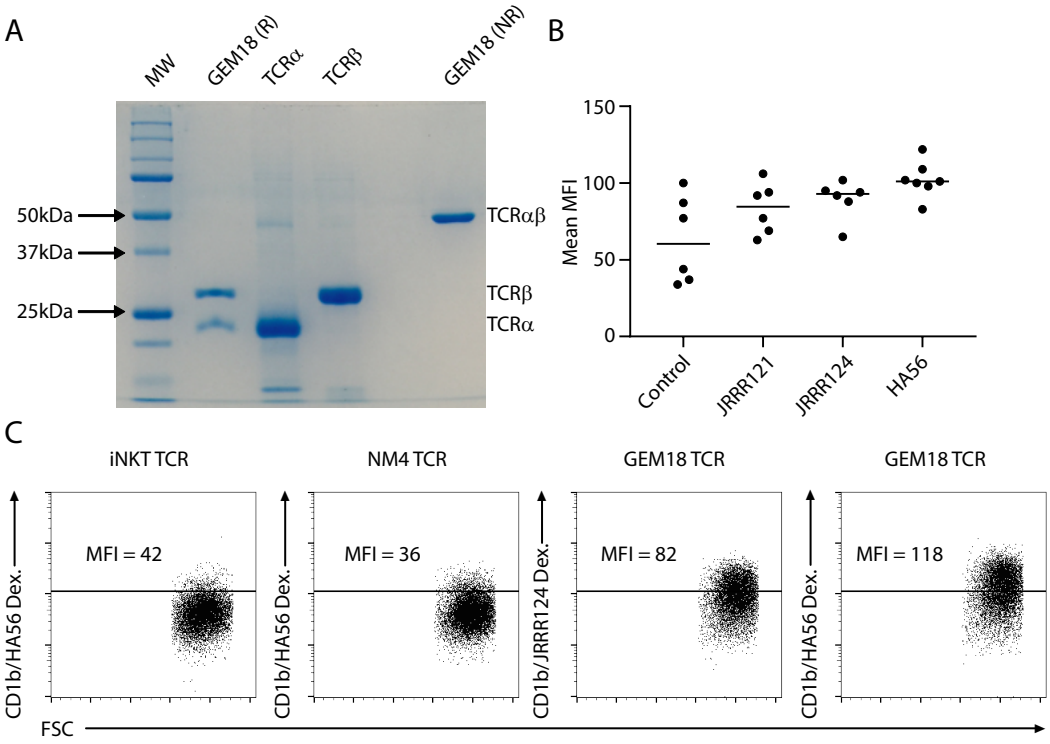
A
MW
GEM18 (R)
TCRα
TCRβ
GEM18 (NR)
50kDa
37kDa
25kDa
TCRαβ
TCRβ
TCRα
B
Mean MFI
150
100
50
0
Control
JRRR121
JRRR124
HA56
C
iNKT TCR
NM4 TCR
GEM18 TCR
GEM18 TCR
MFI = 42
MFI = 36
MFI = 82
MFI = 118
CD1b/HA56 Dex.
CD1b/HA56 Dex.
CD1b/JRRR124 Dex.
CD1b/HA56 Dex.
FSC

A

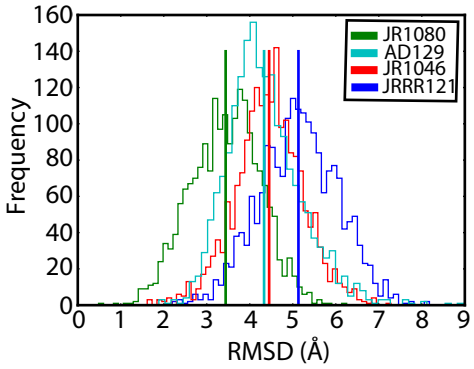
160
140
120
100
80
60
40
20
0
Frequency
0 1 2 3 4 5 6 7 8 9
RMSD (Å)
JR1080
AD129
JR1046
JRRR121

B

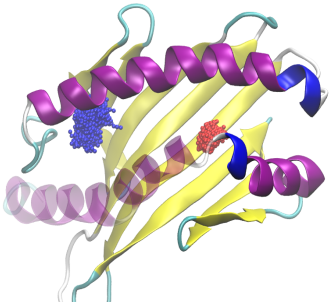

C